NUCL SCI TECH (2021) 32:63
https://doi.org/10.1007/s41365-021-00892-0

Reformatted method for two-dimensional detector arrays measurement data in proton pencil beam scanning

Meng-Ya Guo[1,2] · Xiu-Fang Li[3] · Jie Wang[3] · Qi Liu[1,2] · Xiu-Zhen Deng[1,2] · Man-Zhou Zhang[4] · Li-Ren Shen[4] · Yue-Hu Pu[3,4] · Zhi-Ling Chen[4]

Received: 21 December 2020 / Revised: 1 April 2021 / Accepted: 10 April 2021 / Published online: 16 June 2021

Abstract The spatial resolution of a commercial two-dimensional (2D) ionization chamber (IC) array is limited by the size of the individual detector and the center-to-center distance between sensors. For dose distributions with areas of steep dose gradients, inter-detector dose values are derived by the interpolation of nearby detector readings in the conventional mathematical interpolation of 2D IC array measurements. This may introduce significant errors, particularly in proton spot scanning radiotherapy. In this study, by combining logfile-based reconstructed dose values and detector measurements with the Laplacian pyramid image blending method, a novel method is proposed to obtain a reformatted dose distribution that provides an improved estimation of the delivered dose distribution with high spatial resolution. Meanwhile, the similarity between the measured original data and the downsampled logfile-based reconstructed dose is regarded as the confidence of the reformatted dose distribution. Furthermore, we quantify the performance benefits of this new approach by directly comparing the reformatted dose distributions with 2D IC array detector mathematically interpolated measurements and original low-resolution measurements. The result shows that this new method is better than the mathematical interpolation and achieves gamma pass rates similar to those of the original low-resolution measurements. The reformatted dose distributions generally yield a confidence exceeding 95%.

Keywords 2D ion chamber array detectors · Laplacian pyramid image blending · High-resolution reformatted methods · Pencil beam scanning · Proton therapy

1 Introduction

Proton therapy has become increasingly popular in recent years owing to its advantage in protecting normal tissues beyond tumors [1–3]. The Shanghai Advanced Proton Therapy (SAPT), as a spin-off of the Shanghai Synchrotron Radiation Facility, is currently under commission. The SAPT is installed at the Ruijin Hospital Proton Therapy Center, and clinical trials for the National Medical Products Administration permit will begin soon. All the data presented here were measured in the horizontal beamline of the SAPT.

A pencil beam scanning (PBS) proton delivery system was implemented in the SAPT. A proton pencil beam (also known as a spot) can be delivered to a specified position by changing the magnetic fields and mono-energies based on the treatment plan [4, 5]. Intensity-modulated proton therapy (IMPT) simultaneously optimizes the weights of

✉ Zhi-Ling Chen
chenzl@sari.ac.cn

1 Shanghai Institute of Applied Physics, Chinese Academy of Sciences, Shanghai 201800, China

2 University of Chinese Academy of Sciences, Beijing 100049, China

3 Shanghai APACTRON Particle Equipment Co. Ltd, Shanghai 201800, China

4 Shanghai Advanced Research Institute, Chinese Academy of Sciences, Shanghai 201210, China

thousands of spots for all fields to achieve a good conformal dose distribution in the target volume with a significantly reduced normal tissue dose. Compared with the passive scattering technique based on a single-field uniform dose, the PBS-based IMPT involves more complicated plans and is more sensitive to position disturbances and range uncertainties. Hence, the experimental verification or quality assurance (QA) of treatment plans is important.

For spot scanning, the three-dimensional (3D) dose verification of QA is the optimal option; however, 3D measurement approaches are still in the experimental stage and not yet commercially available [6, 7]. Two-dimensional (2D) dosimetry verification is the mainstream method for patient dosimetric QA for proton radiotherapy. Whereas radiochromic films, such as EBT3 films (Ashland, Bridgewater, NJ, USA) provide high spatial resolution, post-processing is laborious and time-consuming [8]. To improve the efficiency of QA in proton therapy, 2D IC array detectors have been widely used to perform QA verifications. The feasibility of using commercial 2D IC array detectors for proton dose verification, such as MatriXX PT (IBA Dosimetry, Schwarzenbruck, Germany), has been investigated by many researchers [9, 10].

Compared with radiochromic films, 2D IC array detectors provide online measurements and are efficient and convenient. However, owing to the limited resolution of MatriXX PT, 2D detectors cannot provide adequate information in steep dose gradient regions. In a recent study, Brodbek et al. [11] investigated the applicability of 2D detectors in IMPT plans from the perspective of signal processing theory. It was indicated that the detector sampling distances were sufficient to reconstruct the dose distribution in clinical cases with a range shifter, whereas the Nyquist theorem was violated in a planned dose with steep dose gradients, and the measurements did not represent the original dose distribution well. The Nyquist theorem is a concept of the signal processing theory, in which measurements can be used to fully reconstruct the original investigated dataset after the Fourier transform if the sampling frequency is at least twice the maximum frequency of the original dataset. Using a limited number of measurement points whose sampling frequency does not conform to the Nyquist theorem to reconstruct the original dose distribution or interpolations between insufficient measurement points may result in significant errors in some interpolated points in steep dose gradients.

Logfiles record actual information of delivered iso-plane positions of spots, weights, and energies during irradiation, which can be used to reconstruct the logfile-based delivered dose distributions using a dose delivery reconstruction toolkit. The logfile-based reconstructed dose distribution includes dose uncertainties from external factors, such as fluctuations of the accelerator and delivery system. However, in the proton spot scanning delivery system, the spot positions are measured by the strip ionization chamber in the nozzle. This chamber obtains the signal on each strip simultaneously at a certain frequency, and then these data are fitted online to obtain the spot positions. Owing to the limitations of the sampling frequency and the strip width, as well as the misalignment of the strip ionization chamber, submillimeter differences were observed between the measured value and real position [12]. In addition, the beam spot size fluctuated during irradiation, which was not considered in the logfile-based reconstructed dose distribution. Hence, the logfile-based reconstructed dose distribution did not completely coincide with the actual dose distributions.

Therefore, the logfile-based reconstructed dose distribution and 2D IC array detector measurements were combined in this study. Additionally, a method is proposed to obtain a high-resolution reformatted dose distribution without increasing the measurement time and number of equipment, while a few erroneous data points are introduced to compensate for overlooked dose details owing to the large sampling distance of the 2D IC array detectors.

2 Materials and methods

As shown in the flowchart in Fig. 1, the reformatted dose distribution is of high resolution and a better estimation of the delivered dose distribution by data blending the 2D IC detector interpolated measurements and the logfile-based reconstructed dose distribution. To generate high-resolution reformatted dose distributions, three main elements are involved: 2D IC detector array measurements, logfile-based reconstructed dose distributions, and a data blending method. The advantages of the reformatted dose distribution were demonstrated in a water phantom for 2D plane doses at selected depths of different spread-out-Bragg peak (SOBP) box plans. These will be discussed in the following sections.

2.1 Two-dimensional ion chamber array

The IBA MatriXX PT comprises 1020 air-vented parallel plate pixel ion chambers arranged in a 32 × 32 grid with a 7.62 mm center-to-center distance. The sensor of each ion chamber was a cylinder measuring 4.2 mm in diameter and 2 mm in height. The active field size of the MatriXX PT was 24 cm × 24 cm.

Conventional mathematical interpolation is widely used to improve the spatial resolution of the measurements. Although the sampling frequency of the MatriXX PT is sufficient for dose distributions with smooth dose

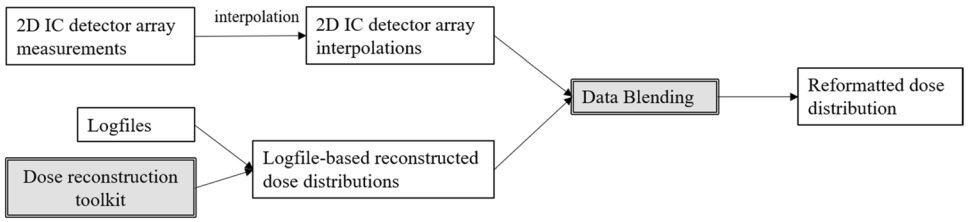

Fig. 1 Flowchart for generating reformative dose distributions

gradients, for dose distributions with more high-frequency components, the interpolation values can deviate significantly from the actual values. Figure 2a shows the measured lateral profiles of a field measuring 10 cm × 10 cm × 10 cm with a range of 20 cm for the treatment plan, and at a depth of 15 cm in the SAPT horizontal beamline. The lateral profile measured based on the EBT3 film exhibited significant dose "horns" at the high gradient edge (indicated by arrows), which is also shown in the calculated dose distribution. The dose "horns" were optimized deliberately to sharpen the lateral fall-off. However, the lateral profile of the interpolated MatriXX PT measurement indicated no "horns" in either edges [13]. Figure 2b shows the Fourier transform of the lateral profile of the planned dose distribution. In signal processing theory, the Nyquist frequency is twice the maximum frequency of the sampled data, and the maximum frequency is defined as the frequency above which all frequency components are below 1% of the maximum amplitude of the Fourier spectrum [11]. In this example, the maximum frequency is 0.0800/mm, which results in a Nyquist frequency of 0.16/mm and a required minimum sampling distance of 6.25 mm. Hence, the minimum sampling distance required is below the sampling distance of MatriXX PT (7.6 mm).

2.2 Dose delivery reconstruction toolkit

Logfile-based reconstructed dose distributions can be reconstructed using a dose delivery reconstruction toolkit with delivered spot positions, weights, and energies recorded in logfiles. Therefore, the accuracy of logfile-based dose distributions directly affects the accuracy of the reformatted dose distributions and is primarily determined by two factors: (1) the input parameters, specifically, the delivered spot positions and weights recorded by logfiles; (2) the dose computation model, which describes the dose deposition in homogeneous or heterogeneous media mathematically. The accuracy of delivered spot positions and weights in logfiles was validated in previous by Liu Ming [14] and Miao Chun Hui [15] in studies pertaining to the SAPT horizontal beamline. The feasibility of dose reconstruction using logfiles in spot scanning proton therapy has been investigated in several proton therapy centers [16, 17]. Regarding the dose computation model, the commissioning of the dose computation model was performed by measuring the integral depth doses and in-air spot size [18, 19]. The dose delivery reconstruction toolkit used was adapted from matRad, which is an open-source software for the radiation treatment planning of intensity-modulated photon, proton, and carbon ion therapy [20]. Many researchers have demonstrated the accuracy of the

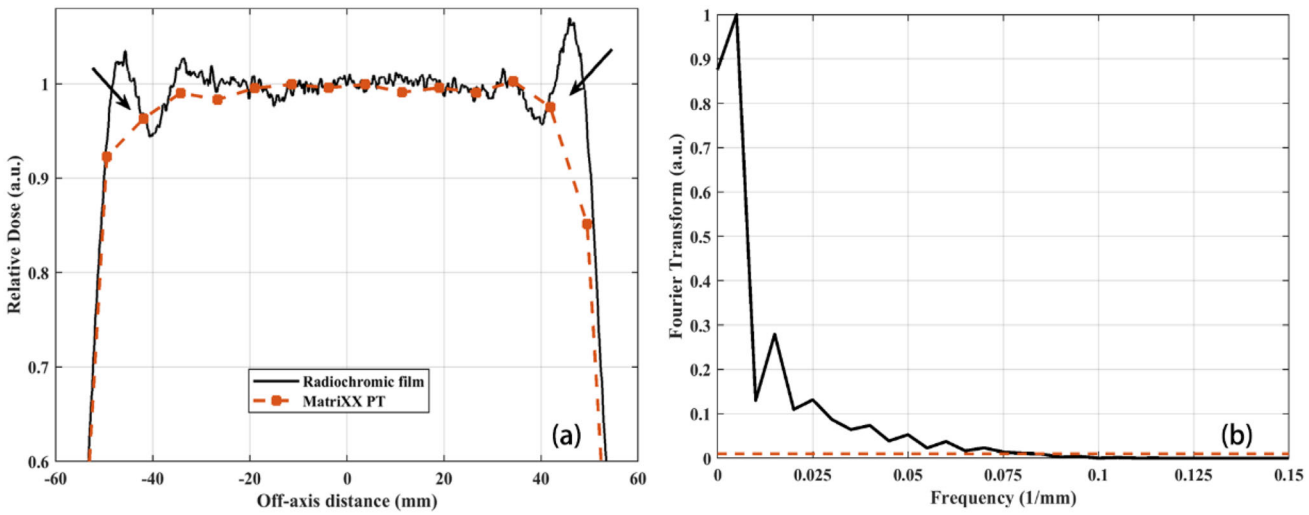

Fig. 2 (Color online) **a** Lateral profiles of field (gantry angle = 270°, couch angle = 0°) of 10 cm × 10 cm × 10 cm treatment plan in 15 cm water equivalent depth measured using EBT3-film, MatriXX PT; **b** corresponding Fourier transform of calculated dose distribution

transportation model in matRad [20, 21], particularly in water. Hence, the main task is to verify the beam modeling.

2.2.1 Verification of dose computation model

It is necessary to validate whether the modeling of pencil beams in the SAPT horizontal beamline for the dose reconstruction toolkit is sufficiently accurate to calculate the delivered dose distributions retrospectively. In contrast to the comparison between the dose based on plans and the measured dose during clinical plan verification, the verification presented herein is based on the comparison of the dose reconstructed by the dose reconstruction toolkit based on logfiles and the film- or Markus-measured data. This verification can eliminate external factors, such as fluctuations of the accelerator and delivery system, and more intuitively reflects the accuracy of the dose computation modeling of the dose reconstruction toolkit. Verification measurements include depth doses along the central axis in several SOBP box plans and lateral dose profiles at various depths of these plans. The SOBP plans (a nominal SOBP width of 6 cm and a range of 10 cm, two nominal SOBP widths of 10 cm, and ranges of 20 or 30 cm) were created using the dose reconstruction toolkit. For the absolute depth dose along the central axis, a calibrated Markus chamber (PTW-Freiburg, Germany) was placed at a selected position in a water phantom during plan delivery. When the current point measurement was completed, the Markus chamber was moved to the next selected position remotely, and the SOBP plan was executed again. In a solid water phantom, EBT3 films were placed at the center of the SOBP flat region to measure the high-resolution relative lateral dose profiles. Three SOBP plans were delivered, and the relevant lateral profiles were measured.

Plans based on clinical cases (prostate cancer and cervical cancer) were delivered, and EBT3 films were placed at depths of 208 and 203 mm in water to measure the 2D relative dose distribution of the corresponding depth.

2.3 Data Blending

2.3.1 Theory

After verifying the accuracy of the independent dose reconstruction toolkit, it can be used to obtain high-resolution reformatted dose distributions and correctly supplement dose details lost from 2D IC array measurements due to low resolution.

In image processing theory and the frequency domain, the low-frequency components of an image are related to the region of slow intensity changes and describe the main part of an image, whereas the high-frequency components of an image correspond to the part with significant intensity changes and indicate the "detailed" part of an image [22]. The proposed method regards 2D dose distributions as images, and "finer" retrospective dose details are blended in with an interpolated measurement dose base to improve the measurement of 2D IC array detectors. Regarding the logfile-based reconstructed dose distribution and the measurement of the 2D IC array detectors, the measurement results are improved by blending the high-frequency components of the logfile-based reconstructed dose images with the low-frequency components of the measured dose images. Laplacian pyramid image blending (LPIB) [23] can blend images smoothly using alpha masks at different frequencies using Laplacian images of different resolutions. Hence, LPIB is a suitable method for blending logfile-based reconstructed and measured dose distributions. The procedures to blend the measured dose and logfile-based reconstructed dose images using LPIB are presented in Fig. 3. Briefly, the procedures are as follows:

(a) Build Laplacian pyramids LP_{p} and LP_{m} from the logfile-based reconstructed dose distribution and the mathematical interpolated measured dose distribution, respectively. The sizes of LP_{p} and LP_{m} at the nth level are $\frac{1}{2}$ of the (n-1)th level. Different LP_{p} and LP_{m} levels represent dose image details for different frequency components.

(b) The alpha mask (AM) is a weight matrix. For the kth level, the hybrid Laplacian pyramid HLP_k from LP_{pk} and LP_{mk} using AM_k as weights is expressed as

$$HLP_k(i,j) = AM_k(i,j) \times LP_{\mathrm{pk}}(i,j) + (1 - AM_k(i,j)) \times LP_{\mathrm{mk}}(i,j),$$

where i and j are the pixel indices. The AM is one of the key parameters for blending logfile-based reconstructed and measured dose distributions, and it reflects the proportion of details of the logfile-based reconstructed dose distribution in the reformatted dose distribution. Furthermore, the AM is determined by the confidence of the reformatted dose distribution, which will be explained later.

(c) The base dose image, i.e., the top image of the Gaussian pyramid of the measured dose distribution, contains the low-frequency information of the measurements. The base dose image describes the main information of the final blended dose distribution. Through the superposition of a base dose image and HLP_k followed by an upsampling, the upsampled dose image $UDI_{k(k-1)}$ with the blended dose details of the kth level is obtained.

(d) Iterate steps b–c for level k-1 to level 1; replace the base dose image by the corresponding $UDI_{(n+1)n}$ during the nth iteration calculation n ($1 < n < k$-1).

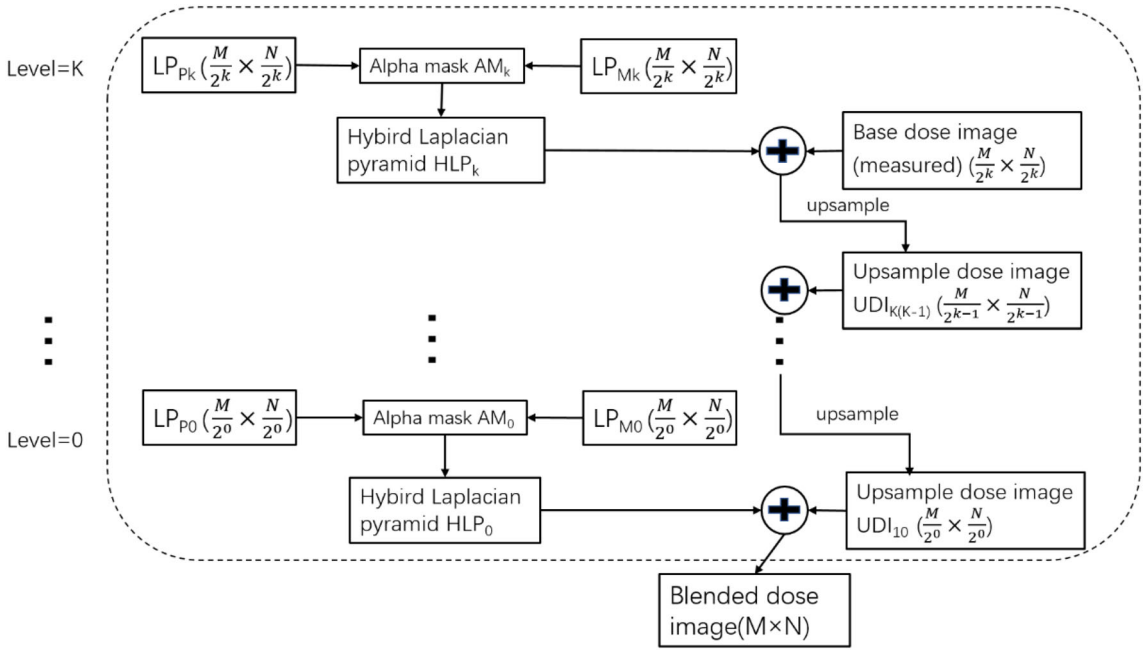

Fig. 3 Flowchart of LPIB method of blending logfile-based reconstructed and measured dose images

(e) Calculate HLP_0 based on step b; superimpose HLP_0 and the upsampling dose image UDI_{10} to obtain the final blended dose image.

In addition, the reformatted dose distribution is a combination of measurements and calculations. Because some factors that can affect the actual dose distribution, such as the fluctuation of the beam spot size, were not considered in the reconstructed dose distributions, the reconstructed dose distributions and actual doses were not exactly identical. Hence, the confidence of the reformatted dose distribution must be evaluated, as it indicates the probability of the reformatted dose distribution representing the true value. The confidence coefficient of the reformatted dose distribution was estimated based on the similarity between the dose distribution of the original low-resolution MatriXX PT measurement and the downsampled logfile-based reconstructed dose distribution. The raw low-resolution measurement data of the MatriXX PT are generally reliable. The difference between the high-resolution interpolated measurement data and the true dose distribution was due to the large sampling distance and insufficient data, which resulted in the interpolation of some error data. Based on the above, for the row measurement as a reference, the more similar the reconstruction dose to the reference, the closer is the reconstruction dose is to the true value. Therefore, the reformatted dose distribution obtained by blending the measured dose with the logfile-based reconstructed dose at high frequencies is more reliable. As such, it is rational to correlate the confidence of the reformatted dose distribution with similarity. Similarity is evaluated based on gamma pass rates [24] in two dimensions with tolerances of 3 mm and 3% of the downsampled logfile-based reconstructed dose distributions and raw measurements.

2.3.2 *Experiments*

Experiments were performed for three different SOBP plans (SOBP plan1: range = 10 cm, width = 6 cm, measured depth = 7 cm; SOBP plan2: range = 20 cm, width = 10 cm, measured depth = 15 cm and 7 cm; SOBP plan3: range = 30 cm, width = 10 cm, measured depth = 25 cm). The 2D dose distributions at different depths of different SOBP plans were measured using the MatriXX PT with an EBT3 film attached to the front surface, and a schematic diagram of the experimental setup is shown in Fig. 4. Film measurements were used as references because of their high resolution. To prove the accuracy of the raw MatriXX PT measurement, the gamma pass rates of the original measurement data (resolution = 7.6 mm) and the downsampled film measurements ($GPR_{DF\&OM}$) were calculated. The corresponding logfile-based reconstructed dose distributions were reconstructed using a dose delivery reconstruction toolkit based on logfiles. Reformatted dose distributions were obtained by blending the interpolation measurements (resolution = 1 mm) and logfile-based reconstructed dose distributions using LPIB with four levels. Furthermore, the confidence was obtained by calculating the gamma pass rates between the original MatriXX PT measurements and the downsampled logfile-

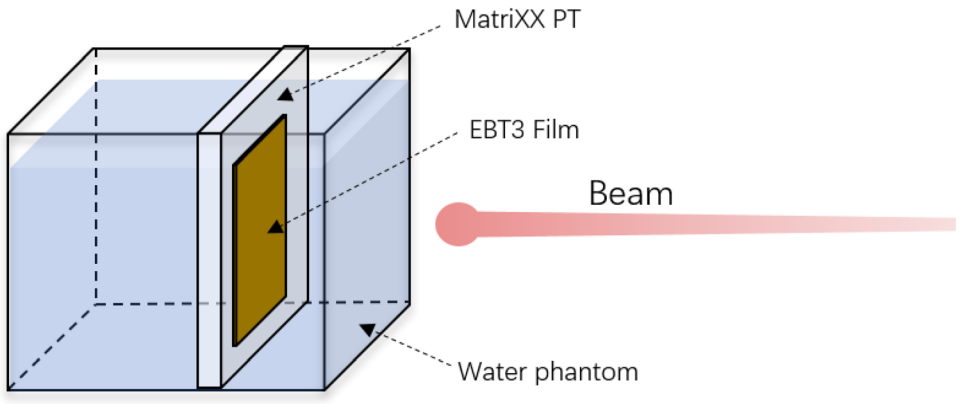

Fig. 4 (Color online) Schematic diagram of experimental setups

based reconstructed dose distributions. To evaluate the accuracy of the reformatted dose distributions, the gamma pass rates between the interpolated MatriXX PT measurements and film dose distributions ($GPR_{F\&IM}$) as well as the gamma pass rates between the reformatted dose distributions and film measurements ($GPR_{F\&R}$) were calculated. The higher the gamma pass rate, the better was the agreement with the actual dose distribution.

3 Results and Discussion

3.1 Verification of dose computation model

Figure 5a shows the measurements and logfile-based reconstructed absolute depth doses along the central axis with three different nominal ranges and widths of SOBP plans. Because the energies used in these plans included high, middle, and low energy sections of the horizontal beamline in the SAPT, these plans were sufficient to verify whether the modeling of energies in this machine system was accurate. Figure 5a shows that the absolute depth doses reconstructed using the dose reconstruction toolkit were consistent with the measured data. As shown in Fig. 5b, the absolute value of percentage differences between the calculated doses based on logfiles and the measured doses at different depths for the three SOBP plans were within 2%, except for the depth of 40 mm in the range of 300 mm of the SOBP plan. The lateral profiles in solid water based on data measured via EBT3 films and data reconstructed by the dose reconstruction toolkit at the center of the three SOBP plans were compared, as shown in Fig. 6a–c. The relative dose lateral profiles of these two datasets demonstrated high consistency in terms of shape and width, particularly in the shoulder areas and 20%–80% of the penumbra. In quantitative analysis, 20%–80% of the penumbra calculated using the dose reconstruction toolkit were consistent with measurements within 0.1 cm, and the

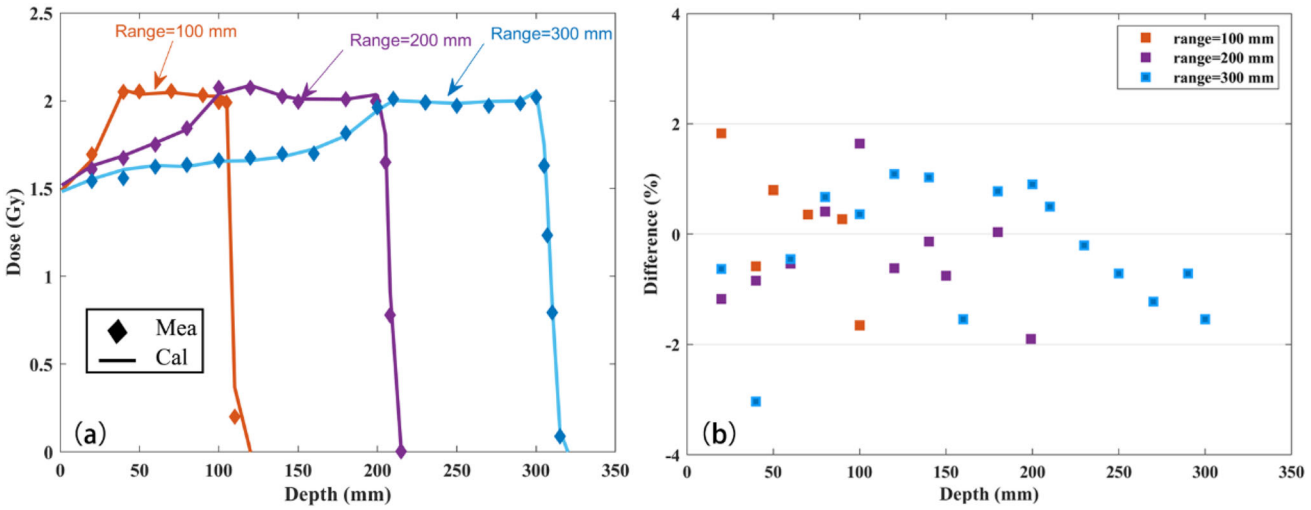

Fig. 5 (Color online) Verification of dose reconstruction toolkit beam modeling in terms of absolute depth dose. **a** Absolute doses of reconstruction and measured doses with depths (diamond represents measured data; solid line represents reconstructed doses). **b** Deviations between reconstructed absolute dose and measured dose at different depths for three plans

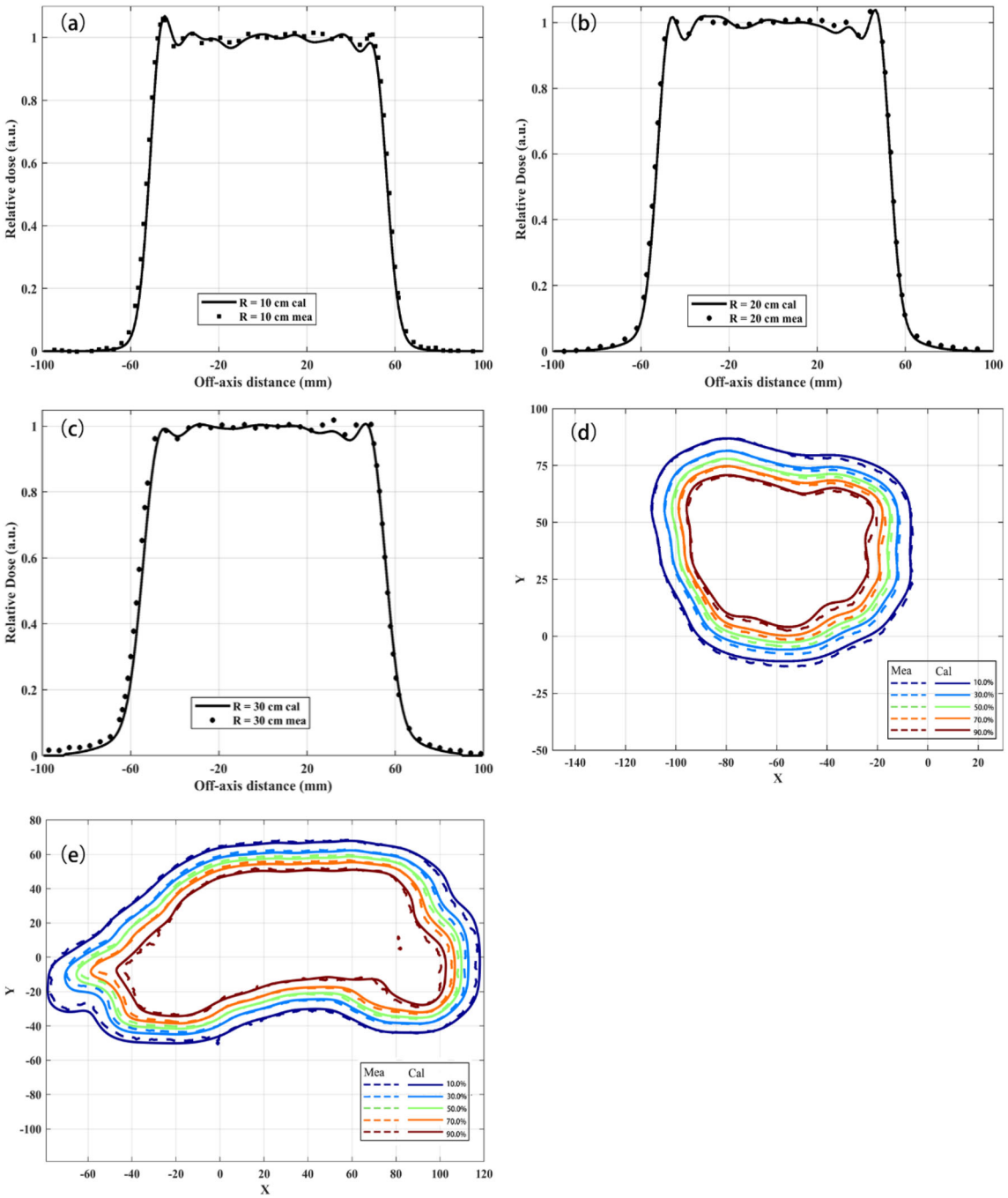

Fig. 6 (Color online) Verification of dose reconstruction toolkit beam modeling in relative 2D dose distribution. **a**–**c** lateral dose profiles at center of three different SOBP plans. **d** Isodose distribution of prostate cancer between film measurement and reconstructed dose distribution. **e** shows isodose distribution of cervical cancer between film measurement and reconstructed dose distribution. **a** Range = 10 cm, SOBP width = 6 cm; **b** range = 20 cm, SOBP width = 10 cm; **c** range = 30 cm, SOBP width = 10 cm

50%–50% field sizes were consistent with the measurements within 0.2 cm.

Figure 6d and 6e shows a comparison of the logfile-based reconstructed dose distributions of the right prostate field at a depth of 20.8 cm and of the right cervical field at a depth of 20.3 cm with the film measured isodose distributions. The logfile-based reconstructed dose distribution agreed well with the film measurement. By comparing the absolute depth doses and relative 2D dose distributions with the measured data, the accuracy of the pencil beam model in this dose reconstruction toolkit can be considered reliable and acceptable.

3.2 Data blending

Figure 7a shows the lateral profiles of the inline of four results (film measurement, logfile-based reconstructed dose distribution, MatriXX PT measurement interpolation, and reformatted dose distribution) at a depth of 150 mm. "Horns" (indicated by arrows) that were not detected due to the low sampling resolution of MatriXX PT appeared in the reformative dose distribution, similar to the film measurement (reference). To clearly show the details of the shoulder areas, Fig. 7a is enlarged, and the start of the longitudinal coordinate was set to 0.6 instead of 0. Although the difference between the logfile-based reconstructed dose and the film dose in the middle of the lateral dose profile was evident, it remained within 3%, as supported by fact that the intensity of the pixel did not exceed 1 in the corresponding position shown in Fig. 7c. Furthermore, many spots with small monitor units (MUs) appeared in the middle of the cube because of the dosimetric superposition of other spots. When the spots with small MUs were delivered, the recorded measurements of position and dose detectors in the nozzle might exhibit some deviations owing to the sampling frequency and sensitivity of the detectors [25]. As shown in Table 1 and Fig. 7a, although the blending weight of the logfile-based reconstructed dose distribution (confidence) was 98.01%, the reformatted lateral profile did not completely coincide with the logfile-based reconstructed dose distribution. This is because the blending weight was only the weight of the detail or high-frequency component blending, and the "main" part (low frequencies) of the reformatted dose distribution was fully derived from the MatriXX PT measurement. This proves that the LPIB method fully utilized the measurement data. Figure 7b shows the gamma index

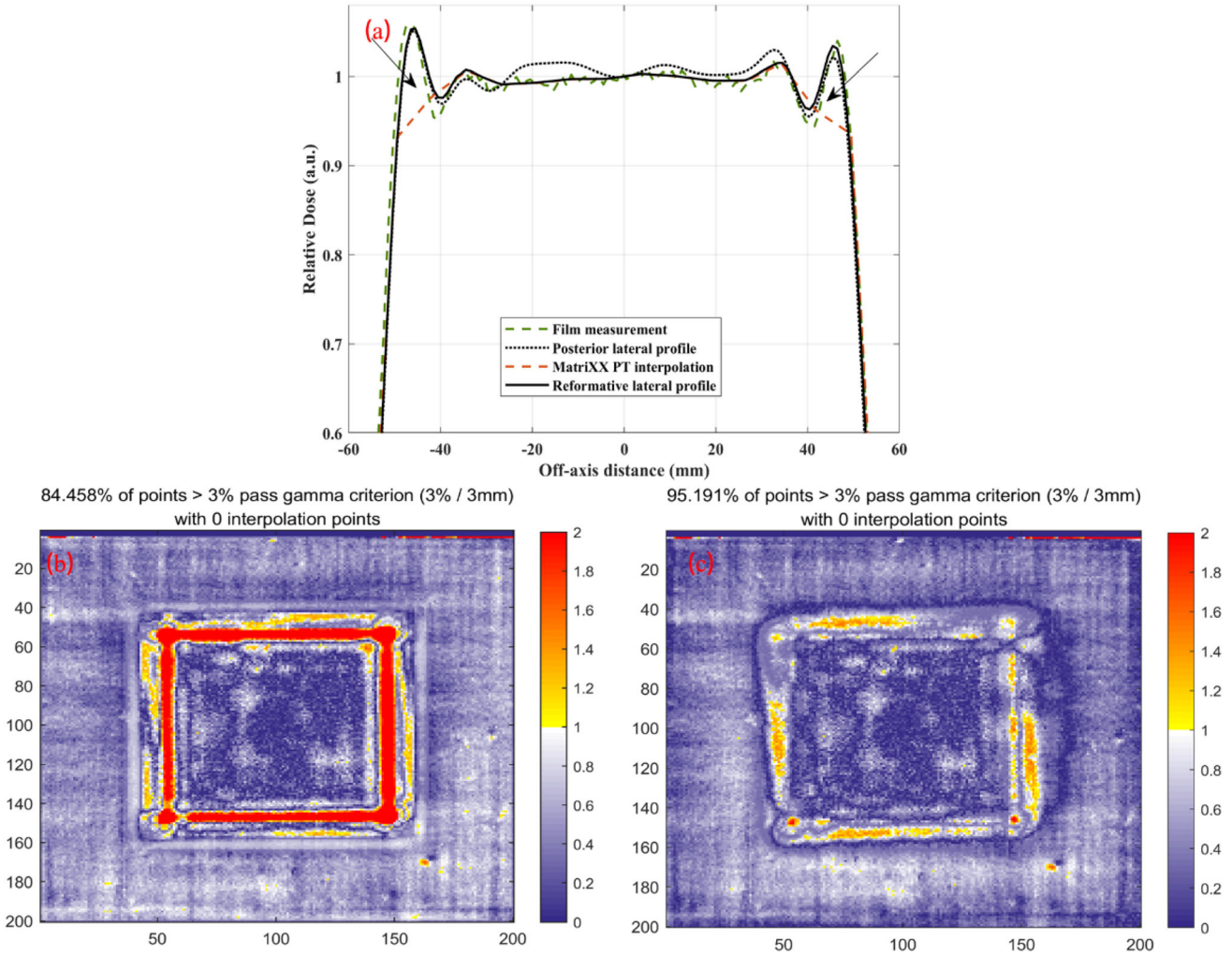

Fig. 7 (Color online) Comparison of reformative dose distribution and original measured dose distribution at depth of 150 mm for range = 200 mm in SOBP plan. **a** Lateral profiles of film measurement, MatriXX PT measurement interpolation, and reformative dose distribution; **b** gamma index distribution between film measurement and MatriXX PT measurement interpolation; **c** gamma index distribution between film measurement and reformative dose distribution

Table 1 Comparison of reformatted dose distributions and interpolated MatriXX PT measurements of different SOBP plans and different depths with gamma pass rates

Number	Plans	Depths (cm)	S_{min} *1 (mm)	$GPR_{DF\&OM}$ *2 (%)	$GPR_{F\&IM}$ *3 (%)	$GPR_{F\&R}$ *4 (%)	C_R *5 (%)
1	1	7	5.88	96.30	87.39	96.34	98.77
2	2	7	4.76	73.24	57.46	81.52	64.44
3	2	15	6.25	96.31	84.46	95.19	98.01
4	3	25	7.69	95.24	98.91	99.96	98.89

*1: minimum required sampling distance; *2: gamma pass rates between downsampled film measurements and 2D IC array original measurements; *3: gamma pass rates between mathematically interpolated 2D IC array detector measurements and film measurements; *4: gamma pass rates between reformatted dose distributions and film measurements; *5: confidence of reformatted dose distribution

distribution of the interpolated MatriXX PT measurement and film measurement; the gamma pass rate was 84.46%. In the gamma index distribution, the closer the pixel intensity is to 0, the better is the dose deviations of the corresponding voxel of the two dose distributions. When the pixel intensity exceeds 1, the dose difference of this voxel between the two dose distributions is unacceptable. Combined with Fig. 7a, it was observed that the differences between these two dose measurements were primarily concentrated on the "horns." Fig. 7c shows the gamma index distribution of the reformatted dose distribution and film measurements. As shown in Fig. 7c, the gamma pass rate increased to 95.19%, and the number of pixels with a gamma index greater than 1 reduced significantly. The pixel intensities of the middle position in Fig. 7c did not exceed 1, thereby proving that the difference between the logfile-based reconstructed dose and the film dose in the middle of the lateral dose profile was acceptable.

A comparison of the reformatted dose distributions and interpolated 2D IC array measurements with the reference dose distribution (film measurement) at different depths for different SOBP plans is shown in Table 1. Most of the gamma pass rates from the downsampled film measurements and 2D IC array original measurements ($GPR_{DF\&OM}$) exceeded 95%, indicating that the raw data measured using MatriXX PT were sufficiently accurate compared with the film measurements. As shown in the third column of Table 1, when the minimum required sampling distance was less than the sampling distance of MatriXX PT (7.6 mm), the gamma pass rates from the mathematically interpolated 2D IC array detector measurements and film measurements ($GPR_{F\&IM}$) were less than 90%, e.g., numbers.1, 2, and 3, which is consistent with the results of Brodbek et al. [11]. Comparing the fifth and sixth columns of Table 1, the gamma pass rates of the reformatted dose distributions demonstrated better agreement with the film measurements than the interpolated 2D IC array measurements. Most of the gamma pass rates from the reformatted dose distributions and film measurements ($GPR_{F\&R}$) exceeded 95%. Moreover, the gamma pass rates shown in the fourth and sixth columns of Table 1 were similar, indicating that the resolution of the MatriXX PT measurements improved with the same accuracy as the original low-resolution measured data. Mathematical interpolation methods cannot achieve such results in dose distributions containing more high-frequency components.

Owing to multiple Coulomb scattering, the dose distribution was more smoothed out at larger depths, as shown by number 4 in Table 1. In most clinical plans, the minimum required sampling distance at these depths is larger; therefore, MatriXX PT measurements can fully reflect the actual dose distribution, and the original $GPR_{F\&IM}$ is typically higher.

In addition to the performance of the monitor chambers, the variation in spot size during irradiation contributed to the deviations between the logfile-based reconstructed dose and delivered dose distributions. Kraan et al.[26] reported that the gamma pass rates of most clinical plans with ± 20% variation in medium spot size cannot achieve 90% with the 2 mm/2% criterion. The threshold of the spot size variation was 15% at the horizontal beamline of the SAPT. The variation in spot size was not considered in the logfile-based reconstructed dose distribution. Furthermore, because the beam spot shape was not round, shape distortion occurred during gantry rotation; this resulted in differences between the logfile-based reconstructed dose and delivered dose distributions, and they were not considered in the logfiles. Hence, for some smooth dose distribution or area, 2D IC array measurements are relatively accurate and can be used to improve the logfile-based reconstructed dose distribution, such as the number 4 and smooth area in Fig. 7a.

The confidence of the reformatted dose distribution was generally greater than 95%, indicating that the reformatted dose distribution can represent the true dose distribution with high probability. However, number 2 was measured at a shallow depth and possessed more high-frequency components. The sampling distance of the 2D IC array was much larger than the minimum required sampling distance,

and many details were lost in the 2D IC detector measurement. In general, provided that the dose computation model for the pencil beam is correct, the logfile-based reconstructed dose distribution will exhibit better consistency with the actual distribution. Hence, the gamma pass rates of the original 2D IC detector measurement and the downsampled logfile-based reconstructed dose distribution were low, thereby resulting in a low confidence coefficient.

In data blending, the AM is determined by the confidence of the reformatted dose distribution, which is the similarity between the original measurement and the downsampled logfile-based reconstructed dose distribution. Compared with treatment plans with smooth dose distributions, owing to the low sampling rate of MatriXX PT and the dose response of a single sensor, the similarities between the raw measurements and the downsampled logfile-based reconstructed dose distributions of treatment plans with more high-frequency components were lower. Therefore, the proportion of the logfile-based reconstructed dose distribution in the blended data was smaller, and the reformatted dose distribution was not consistent with the actual data, such as Number 2. By contrast, for a smooth dose distribution, the proportion of the logfile-based reconstructed dose distribution in the reformatted dose distribution was large. Therefore, the use of confidence as an AM limits the improvement of measured dose distributions with extremely steep gradient areas.

Another essential parameter in LPIB is the number of pyramid levels, which affects the proportion of measured data in the reformatted dose distribution. When the number of pyramid levels is between 1 and 3, the logfile-based reconstructed dose distribution accounts for extremely small weights, the improvement in the measurement part that is overlooked due to low resolution is less, and the reformatted effect is not significant. When the number of pyramid levels exceeds five, the measured data account for a small proportion, which violates our intention to fully utilize the data. When the number of pyramid levels is four, the proportions of the logfile-based reconstructed dose distribution and the measured data are balanced.

Regarding the experiments performed in this study, the number of plans for clinical cases is few, and these plans are not challenging. This study lacks plans based on clinical cases that involve many organs at risk such as nasopharyngeal cancer or superficial tumors such as breast cancer. However, we believe that, with subsequent clinical testing for the horizontal beamline in the SAPT, more clinical case plans will be established to support the conclusion presented herein. Furthermore, because MatriXX PT does not perform absolute dose calibration in the SAPT, all measured and reformatted dose distributions are relative values. It is believed that LPIB demonstrates greater potential for absolute dose improvement.

4 Conclusion

To obtain high-resolution reformatted dose distributions of 2D IC array detector measurements for patient QA in proton pencil beam spot scanning, a method of blending low-frequency components of the measurement and high-frequency components of the logfile-based reconstructed dose through LPIB is proposed. The accuracy of the dose calculation model in the dose calculation toolkit for calculating the logfile-based reconstructed dose distributions was verified. This method compensates for details that were overlooked owing to the low sampling rate of the detectors, and the reformatted dose distribution indicated better agreement with the film measurements compared with the traditional interpolated dose method.

Acknowledgment The authors would like to thank colleagues from Shanghai APACTRON Particle Equipment Co., Ltd. for their skillful operation of the treatment facility. We would also like to express our gratitude to medical physicists from the Department of Radiation Oncology, Shanghai Ruijin Hospital for their clinical advice and assistance with the data.

Author contributions All authors contributed to the study conception and design. Material preparation, data collection, and analysis were performed by Meng-Ya Guo, Xiu-Fang Li, and Jie Wang. The first draft of the manuscript was written by Meng-Ya Guo and all authors commented on previous versions of the manuscript. All authors read and approved the final manuscript.

References

1. R. Pidikiti, B.C. Patel, M.R. Maynard et al., Commissioning of the world's first compact pencil-beam scanning proton therapy system. J. Appl. Clin. Med. Phys. **19**, 94–105 (2018). https://doi.org/10.1002/acm2.12225
2. H. Sakurai, H. Ishikawa, T. Okumura, Proton beam therapy in Japan: current and future status. Jap. J. Clinical Oncol. **46**, 885–892 (2016). https://doi.org/10.1093/jjco/hyw102
3. J. Doyen, P.Y. Bondiau, K. Benezery et al., Current situation and perspectives of proton therapy. Cancer Radiotherapie. **19**, 211–219 (2015). https://doi.org/10.1016/j.canrad.2014.12.010
4. E. Pedroni, R. Bacher, H. Blattmann et al., The 200-MeV proton therapy project at the Paul Scherrer Institute: conceptual design and practical realization. Med. Phys. **22**, 37–53 (1995). https://doi.org/10.1118/1.597522
5. A. Lomax, T. Bohringer, A. Bolsi et al., Treatment planning and verification of proton therapy using spot scanning initial experience. Med. Phys. **31**, 3150–3157 (2004). https://doi.org/10.1118/1.1779371
6. S. Safai, S.X. Lin, E. Pedroni, Development of an inorganic scintillating mixture for proton beam verification dosimetry. Phys. Med. Biol. **49**, 4637–4655 (2004). https://doi.org/10.1088/0031-9155/49/19/013
7. F. Kroll, J. Pawelke, L. Karsch, Preliminary investigations on the determination of three-dimensional dose distributions using scintillator blocks and optical tomography. Med. Phys. **40**, 082104 (2013). https://doi.org/10.1118/1.4813898
8. M.F. Chan, C.-C. Chen, C. Shi et al., Patient-Specific QA of Spot-Scanning Proton Beams using Radiochromic Film,

International journal of medical physics. Clin. Eng. Radiat. Oncol. **6**, 111–123 (2017). https://doi.org/10.4236/ijmpcero.2017.62011

9. B. Arjomandy, N. Sahoo, G. Ciangaru et al., Verification of patient-specific dose distributions in proton therapy using a commercial two-dimensional ion chamber array. Med. Phys. **37**, 5831–5837 (2010). https://doi.org/10.1118/1.3505011
10. B. Arjomandy, N. Sahoo, X.N. Ding et al., Use of a two-dimensional ionization chamber array for proton therapy beam quality assurance. Med. Phys. **35**, 3889–3894 (2008). https://doi.org/10.1118/1.2963990
11. L. Brodbek, J. Kretschmer, K. Willborn et al., Analysis of the applicability of two-dimensional detector arrays in terms of sampling rate and detector size to verify scanned intensity-modulated proton therapy plans. Med. Phys. **47**, 4589–4601 (2020). https://doi.org/10.1002/mp.14346
12. N.S.H. Li, F. Poenisch, K. Suzuki et al., Use of treatment log files in spot scanning proton therapy as part of patient-specific quality assurance. Med. Phys. **40**, 021703 (2013). https://doi.org/10.1118/1.4773312]
13. C. Winterhalter, A. Lomax, D. Oxley et al., A study of lateral fall-off (penumbra) optimisation for pencil beam scanning (PBS) proton therapy. Phys. Med. Biol. **63**, 025022 (2018). https://doi.org/10.1088/1361-6560/aaa2ad
14. M. Liu, H. Zhang, H. Shu et al., Technical commissioning of the spot scanning system in Shanghai Proton Therapy Facility. Rad. Det. Technol. Meth. **4**, 46–55 (2019). https://doi.org/10.1007/s41605-019-0148-5
15. C.-H. Miao, M. Liu, C.-X. Yin et al., Precise magnetic field control of the scanning magnets for the APTRON beam delivery system. Nucl. Sci. Tech. **28**, 172 (2017). https://doi.org/10.1007/s41365-017-0324-6
16. H. Li, N. Sahoo, F. Poenisch et al., Use of treatment log files in spot scanning proton therapy as part of patient-specific quality assurance. Med. Phys. **40**, 021703 (2013). https://doi.org/10.1118/1.4773312
17. M.F. Belosi, R. van der Meer, P. Garciade Acilu Laa et al., Treatment log files as a tool to identify treatment plan sensitivity to inaccuracies in scanned proton beam delivery. Radiother Oncol. **125**, 514–519 (2017). https://doi.org/10.1016/j.radonc.2017.09.037
18. M.T. Gillin, N. Sahoo, M. Bues et al., Commissioning of the discrete spot scanning proton beam delivery system at the University of Texas MD Anderson Cancer Center, Proton Therapy Center, Houston. Med. Phys. **37**, 154–163 (2010). https://doi.org/10.1118/1.3259742
19. X.R. Zhu, F. Poenisch, M. Lii et al., Commissioning dose computation models for spot scanning proton beams in water for a commercially available treatment planning system. Med. Phys. **40**, 041723 (2013). https://doi.org/10.1118/1.4798229
20. H.P. Wieser, E. Cisternas, N. Wahl et al., Development of the open-source dose calculation and optimization toolkit matRad. Med. Phys. **44**, 2556–2568 (2017). https://doi.org/10.1002/mp.12251
21. E. Cisternas, A. Mairani, P. Ziegenhein et al., in *MatRad - a multi-modality open source 3D treatment planning toolkit*, ed. by D. Jaffray. World Congress on Medical Physics and Biomedical Engineering, June 7-12, 2015, Toronto, Canada. IFMBE Proceedings, vol 51 (Springer, Cham, 2015). https://doi.org/10.1007/978-3-319-19387-8_391
22. R.C. Gonzales, R.E. Woods, S.L. Eddins, *Digital Image Processing* (Prentice Hall, Upper Saddle River, NJ, 2008)
23. P.J. Burt, E.H. Adelson, The laplacian pyramid as a compact image code. IEEE Trans. Commun. **31**, 532–540 (1983). https://doi.org/10.1109/tcom.1983.1095851
24. A.D. Low, W.B. Harms, S. Mutic et al., A technique for the quantitative evaluation of dose distributions. Med. Phys. **25**, 656–661 (1998). https://doi.org/10.1118/1.598248
25. R.-C. Han, Y.-J. Li, Y.-H. Pu, Collection efficiency of a monitor parallel plate ionization chamber for pencil beam scanning proton therapy. Nucl. Sci. Tech. **31**, 13 (2020). https://doi.org/10.1007/s41365-020-0722-z
26. A.C. Kraan, N. Depauw, B. Clasie et al., Impact of spot size variations on dose in scanned proton beam therapy. Phys. Med. **57**, 58–64 (2019). https://doi.org/10.1016/j.ejmp.2018.12.011